

# Non-Hermitian topological phases and dynamical quantum phase transitions: a generic connection

Longwen Zhou<sup>1,\*</sup> and Qianqian Du<sup>1</sup>

<sup>1</sup>*Department of Physics, College of Information Science and Engineering,  
Ocean University of China, Qingdao, China 266100*

(Dated: 2021-06-18)

## Abstract

The dynamical and topological properties of non-Hermitian systems have attracted great attention in recent years. In this work, we establish an intrinsic connection between two classes of intriguing phenomena – topological phases and dynamical quantum phase transitions (DQPTs) – in non-Hermitian systems. Focusing on one-dimensional models with chiral symmetry, we find DQPTs following the quench from a trivial to a non-Hermitian topological phase. Moreover, the critical momenta and critical time of the DQPTs are found to be directly related to the topological invariants of the non-Hermitian system. We further demonstrate our theory in three prototypical non-Hermitian lattice models, the lossy Kitaev chain (LKC), the LKC with next-nearest-neighbor hoppings, and the nonreciprocal Su-Schrieffer-Heeger model. Finally, we suggest a proposal to experimentally verify the found connection by a nitrogen-vacancy center in diamond.

arXiv:2102.07116v2 [quant-ph] 17 Jun 2021

---

\* zhoulw13@u.nus.edu

## I. INTRODUCTION

Non-Hermitian systems have attracted great interest in recent years due to their intriguing dynamical and topological properties [1–8]. Theoretically, exceptional point (EP) induced chiral dynamics [9–11] and non-Hermitian topological matter [12–15] have been found and explored in a variety of systems. Experimentally, non-Hermitian topological phases and phenomena have been observed in cold atom [16–18], photonic [19–22], electric circuit [23–25], acoustic [26–28] systems and nitrogen-vacancy-center in diamond [29, 30], leading to potential applications like unidirectional transport devices [31, 32], topological lasers [33–35] and high-performance sensors [36–39].

To date, non-Hermitian topological phases (NHTPs) have been classified and characterized according to their protecting symmetries [13–15]. Finding the dynamical signatures of these nonequilibrium topological matter has become an urgent topic for further theoretical and experimental explorations. In the literature, several dynamical probes to the topological invariants of one- and two-dimensional non-Hermitian phases have been proposed, such as the non-Hermitian extension of mean chiral displacements [40–42] and dynamical winding numbers [43–46]. In the meantime, DQPTs (i.e., nonanalytic behaviors of certain observables in time domain [48–51]) following a quench across the EPs of a non-Hermitian lattice model is investigated in Ref. [52], and the monotonic growth of a dynamical topological order parameter in time is observed if an isolated EP is crossed during the quench [52]. This discovery indicates an underlying relationship between the two notably different nonequilibrium phenomena, NHTPs and DQPTs. However, the more general connection between NHTPs and DQPTs, together with its possible experimental observations have not been revealed.

In this work, we uncover an intrinsic connection between the topological phases and DQPTs in one-dimensional (1D) non-Hermitian systems. In Sec. II, we develop our theoretical framework leading to the establishment of this connection. In Sec. III, we demonstrate the found connection in three different non-Hermitian lattice models, the lossy Kitaev chain (LKC), the LKC with next-nearest-neighbor (NNN) hoppings and pairings, and the non-reciprocal Su-Schrieffer-Heeger (NRSSH) model. In each model, a direct link between the bulk topological invariant of a non-Hermitian phase and the number of critical time and momenta of DQPTs following a quench to the corresponding phase is found. In Sec. IV, we

discuss an experimental setup, the nitrogen-vacancy (NV) center in diamond, in which the discovered connection may be tested. We conclude this work and discuss potential future directions in Sec. V.

## II. THEORY

In this section, we introduce a generic class of non-Hermitian lattice models and describing the topological characterization of its bulk states in Subsec. II A. In Subsec. II B, we introduce relevant quantities to characterize DQPTs in 1D non-Hermitian systems, and establish their connections with the underlying topological properties of the system.

### A. NHTPs

We start with a non-Hermitian Hamiltonian  $H \neq H^\dagger$ , which describes particles in a 1D lattice subjecting to gains, losses and/or nonreciprocal effects. Under the periodic boundary condition, we can express the Hamiltonian of the system as  $H = \sum_k \Psi_k^\dagger H(k) \Psi_k$ , where  $k \in [-\pi, \pi)$  is the quasimomentum,  $\Psi_k^\dagger$  ( $\Psi_k$ ) is the two-component creation (annihilation) operator in momentum representation, and the Bloch Hamiltonian  $H(k)$  takes the general form

$$H(k) = [h_a(k) - ig_a(k)]\sigma_a + [h_b(k) - ig_b(k)]\sigma_b. \quad (1)$$

Here  $h_{a,b}(k)$  and  $g_{a,b}(k)$  are real-valued functions of the quasimomentum  $k$ ,  $i$  denotes the imaginary unit, and  $\sigma_{a,b}$  are any two of the three Pauli matrices  $\sigma_x$ ,  $\sigma_y$ , and  $\sigma_z$ , with  $\{\sigma_a, \sigma_b\} = 0$  for  $a \neq b$ . We will also denote the  $2 \times 2$  identity matrix as  $\sigma_0$ .

The non-Hermiticity of  $H$  implies that  $H(k) \neq H^\dagger(k)$  at a generic quasimomentum  $k$ . The dispersion relation of non-Hermitian Bloch Hamiltonian  $H(k)$  is given by

$$\begin{aligned} E_\pm(k) &= \pm \sqrt{[h_a(k) - ig_a(k)]^2 + [h_b(k) - ig_b(k)]^2} \\ &= \pm E(k). \end{aligned} \quad (2)$$

It is clear that  $\pm E(k)$  are in general complex numbers. The spectrum of  $H(k)$  becomes gapless at zero energy if  $E(k) = 0$ . According to Eq. (2), this is achieved when both the

following conditions are satisfied

$$h_a^2(k) + h_b^2(k) - g_a^2(k) - g_b^2(k) = 0, \quad (3)$$

$$h_a(k)g_a(k) + h_b(k)g_b(k) = 0. \quad (4)$$

By solving these equations, we could obtain the quasimomentum  $k_0$  at which the spectrum gap closes, and find the boundaries separating different gapped phases in the parameter space, which could also be the boundaries among different bulk topological phases of the system.

To characterize the topological properties of the gapped phases of  $H(k)$  (i.e.,  $E(k) \neq 0$  for all  $k$ ), the usual recipe is to identify the symmetries of the system and construct the relevant topological invariants. From the commutation relation of Pauli matrices  $[\sigma_a, \sigma_b] = 2i\epsilon_{abc}\sigma_c$ , it is clear that the  $H(k)$  in Eq. (1) possesses the chiral (sublattice) symmetry  $\mathcal{S} = \sigma_c$  ( $c \neq a, b$ ), in the sense that  $\mathcal{S}^2 = \sigma_0$  and  $\mathcal{S}H(k)\mathcal{S} = -H(k)$ . The bulk topological phases of a non-Hermitian Bloch Hamiltonian with sublattice symmetry  $\mathcal{S}$  can usually be characterized by a winding number  $w$ , defined as

$$w = \int_{-\pi}^{\pi} \frac{dk}{2\pi} \partial_k \phi(k), \quad \phi(k) \equiv \arctan \left[ \frac{h_b(k) - ig_b(k)}{h_a(k) - ig_a(k)} \right], \quad (5)$$

which describes the accumulated change of winding angle  $\phi(k)$  throughout the first Brillouin zone (BZ). Note that the value of  $w$  is always real even though  $\phi(k)$  is in general complex, as the imaginary part of  $\phi(k)$  has no winding in the first BZ (see Ref. [43] for a proof). Furthermore, the  $w$  as defined in Eq. (5) can take either integer or half-integer values, depending on the relative locations between the EPs of  $H(k)$  on the  $h_a$ - $h_b$  plane and the trajectory of vector  $\mathbf{h}(k) = [h_a(k), h_b(k)]$  versus  $k$ . That is, if  $\mathbf{h}(k)$  encircles an even (odd) number of EPs, we would have  $w \in \mathbb{Z}$  ( $w \in (2\mathbb{Z} + 1)/2$ ) [43]. Within a gapped topological phase of  $H(k)$ , the value of  $w$  is a constant, whereas it takes a quantized (or half-quantized jump) when a phase boundary determined by Eqs. (3)-(4) is crossed. Therefore, the invariant  $w$  yields a characterization for all the bulk non-Hermitian topological phases of  $H(k)$ . Experimentally, the winding number  $w$  can be obtained by measuring the mean chiral displacements of wave packets [40] or the dynamical winding numbers of time-averaged spin textures [43].

## B. DQPTs and their relations to NHTPs

DQPTs are characterized by nonanalytic behaviors of system observables as functions of time. They are usually found in the dynamics following a quench across the equilibrium phase transition point of a quantum many-body system (see Ref. [48–51] for reviews). The central object in the description of DQPTs is the return amplitude  $G(t) = \langle \Psi | U(t) | \Psi \rangle$ , where  $|\Psi\rangle$  is the initial many-particle state (usually taken as the equilibrium ground state of the system before the quench) and  $U(t)$  is the evolution operator of the system following a quantum quench (or some other nonequilibrium protocols). Formally,  $G(t)$  mimics the dynamical partition function of the post-quench evolution. When  $G(t) = 0$  at a critical time  $t_c$ , the initial state evolves into its orthogonal state. The rate function of return probability  $g(t) = -\lim_{N \rightarrow \infty} N^{-1} \ln |G(t)|^2$  ( $N$  is the number of degrees of freedom of the system) or its time derivatives would then become nonanalytic at  $t = t_c$ , signifying a DQPT. Accompanying theoretical discoveries [53–55], DQPTs have been observed in cold atoms [56–59], trapped ions [60, 61], superconducting qubits [62], nanomechanical and photonic systems [63–65]. Recent studies further extend DQPTs to periodically driven (Floquet) systems [66–71], accompanied by an experimental realization in the NV center setup [66].

To relate DQPTs with topological phases in non-Hermitian systems, we focus on a unique class of quench protocol, in which the system is initialized with equal populations but no coherence on the two bands of the non-Hermitian Bloch Hamiltonian  $H(k)$  in Eq. (1), i.e., an infinite-temperature initial state  $\prod_{k \in \text{BZ}} \rho_0$ , with  $\rho_0 = \sigma_0/2$  being the single-particle density matrix. The evolution of  $\rho_0$  at time  $t > 0$  is governed by  $H(k)$ , and the return amplitude  $G(k, t)$ , defined as the expectation value of evolution operator  $U(k, t) = e^{-iH(k)t}$  over the initial state  $\rho_0$  reads

$$G(k, t) = \text{Tr}[\rho_0 U(k, t)] = \cos[E(k)t], \quad (6)$$

where Eqs. (1) and (2) have been used to reach the second equality. When possible DQPTs happen, we would have  $\cos[E(k)t] = 0$ , leading to the critical times

$$t_n(k) = \left(n - \frac{1}{2}\right) \frac{\pi}{E(k)}, \quad n \in \mathbb{Z}. \quad (7)$$

This seemingly innocent expression yields rather different predictions for Hermitian and non-Hermitian systems. In a Hermitian system, where the dispersion relation  $E(k)$  is always real

and positive, we would have a set of critical times  $t_n(k)$  for each quasimomentum  $k$ . However, the resulting non-analyticity in the rate function  $g(t)$  is simply originated from the oscillatory dynamics of a single Bloch state rather than an actual phase transition, which only happens in thermodynamic limit ( $N \rightarrow \infty$ ). On the other hand, when  $H(k)$  is non-Hermitian, we have  $E(k) \in \mathbb{C}$  in general, and real critical times  $t_n(k)$  emerge only at the critical momenta  $k_c$  where  $E(k_c) \in \mathbb{R}$ . According to Eq. (2), this is equivalent to the fulfillment of the following two conditions:

$$h_a^2(k) + h_b^2(k) - g_a^2(k) - g_b^2(k) > 0, \quad (8)$$

$$h_a(k)g_a(k) + h_b(k)g_b(k) = 0, \quad (9)$$

which only yield solutions at isolated values of  $k$ . For a critical momentum  $k_c$  satisfying both the Eqs. (8) and (9), we would have  $G(k_c, t_n) = 0$  for all  $n \in \mathbb{Z}$ . In the thermodynamic limit, the rate function of return probability for the many-particle initial state  $\prod_{k \in \text{BZ}} \rho_0$  is given by

$$g(t) = - \lim_{N \rightarrow \infty} \frac{1}{N} \ln |G(k, t)|^2 = - \int_{\text{BZ}} \frac{dk}{2\pi} \ln |G(k, t)|^2, \quad (10)$$

which will have discontinuous first-order time derivatives at all  $t_n(k_c)$ . Note that by taking the limit  $N \rightarrow \infty$ , the distribution of  $t_n(k)$  on the complex time plane changes from isolated points to a continuous line, whose crossings along the real-time axis correspond to the critical time of genuine DQPTs in the sense of Fisher zeros [48].

The connection between DQPTs and NHTPs in chiral-symmetric 1D systems becomes transparent at this stage. First, we note that the Eq. (4), which determines the gapless quasimomenta  $\{k_0\}$  is identical to Eq. (9). This implies that the critical momenta  $\{k_c\}$  of DQPTs can only be a subset of  $\{k_0\}$ . Second, plugging  $\{k_0\}$  into Eq. (3), we obtain an expression for the boundaries separating different NHTPs in the parameter space. Combining this with Eq. (8) further suggests that DQPTs can only be observed in certain regimes that are distinguished from the others by the topological phase boundaries of  $H(k)$ . Third, since the number of gapless quasimomenta  $k_0$  is closely related to the change of topological invariant  $w$  in Eq. (5) across the corresponding topological phase transition point, DQPTs with different numbers of  $k_c$  are expected to happen following quenches to different NHTPs. As each critical momentum  $k_c$  determines a unique period  $T(k_c) = \pi/E(k_c)$  for the DQPTs,

the number of critical period  $T(k_c)$  is determined by the number of distinct critical momenta. The third point then suggests a way to distinguish different NHTPs through the quantitative difference of the critical time-periods of DQPTs therein.

Putting together, we have uncovered an intrinsic relation between the topological phases and DQPTs in non-Hermitian systems, which not only bridges the gap between these two diverse fields, but also provides a way to probe the NHTPs through nonequilibrium dynamics. To make the connection more explicit, we will study the DQPTs in a couple of prototypical 1D non-Hermitian lattice models in the following section. Besides the rate function  $g(t)$ , we will also investigate the real-valued, noncyclic geometric phase of the return amplitude  $G(k, t)$  [52], which is defined as

$$\Phi_G(k, t) = \Phi(k, t) - \Phi_D(k, t), \quad (11)$$

where the total phase

$$\Phi(k, t) \equiv -i \ln \frac{G(k, t)}{|G(k, t)|}, \quad (12)$$

and the dynamical phase

$$\Phi_D(k, t) \equiv - \int_0^t dt' \text{Re} \left\{ \frac{\text{Tr}[\tilde{U}^\dagger(k, t') \rho_0 U(k, t') H(k)]}{\text{Tr}[\tilde{U}^\dagger(k, t') \rho_0 U(k, t')]} \right\} \quad (13)$$

(see Appendix A for more details about these phase factors). The noncyclic geometric phase has been shown to contain important information about DQPTs in both Hermitian [72–76] and non-Hermitian [52] systems. At a given time, the winding number of the geometric phase in the first BZ can be further employed to construct a dynamical topological order parameter (DTOP), which is defined as

$$\nu(t) = \int \frac{dk}{2\pi} \partial_k \Phi_G(k, t). \quad (14)$$

It takes a quantized jump whenever the evolution of the system passes through a critical time of the DQPT. Note that the range of integration over  $k$  depends on the symmetry of  $\Phi_G(k, t)$  in  $k$ -space. For example, if  $\Phi_G(k, t)$  has the inversion symmetry with respect to  $k = 0$ , i.e.,  $\Phi_G(k, t) = \Phi_G(-k, t)$ , we can perform the integral over a reduced BZ with  $k \in [0, \pi]$  in the evaluation of  $\nu$  in Eq. (14).

### III. MODELS AND RESULTS

In this section, we demonstrate the connection between NHTPs and DQPTs in three typical non-Hermitian 1D lattice models. In each subsection, we introduce the model that will be investigated first and establish its bulk topological phase diagram. After that, we consider the DQPTs in the model following the quench from a trivial phase to different non-Hermitian phases (either trivial or topological), and unveil the relationship between the critical times and momenta of the DQPTs and the topological invariants of the post-quench non-Hermitian system. In the lossy Kitaev chain and its next-nearest-neighbor extension, we observe a one-to-one correspondence between the NHTPs and DQPTs. In the nonreciprocal SSH model, we find that while a topologically nontrivial post-quench system always imply DQPTs following the quench, the reverse may not be true in general, and possible reasons behind such an anomaly will be discussed.

#### A. The lossy Kitaev chain

We first consider a non-Hermitian variant of the Kitaev chain, which describes a 1D topological superconductor with onsite particle loss. In momentum representation, the Hamiltonian of the model takes the form  $H = \frac{1}{2} \sum_{k \in \text{BZ}} \Psi_k^\dagger H(k) \Psi_k$ , where  $\Psi_k^\dagger = (c_k^\dagger, c_{-k})$  is the Nambu spinor operator and  $c_k^\dagger$  is the creation operator of an electron with quasimomentum  $k$ . The Bloch Hamiltonian  $H(k)$  in Nambu basis is given by

$$H(k) = h_y(k)\sigma_y + [h_z(k) - iv]\sigma_z, \quad (15)$$

where

$$h_y(k) = \Delta \sin k, \quad h_z(k) = u + J \cos k. \quad (16)$$

Here the real parameters  $J$ ,  $\Delta$  and  $u$  denote the nearest-neighbor hopping amplitude, superconducting pairing amplitude and chemical potential.  $v \in \mathbb{R}$  characterizes the strength of onsite particle loss. Following the discussions of Subsec. II A, we see that  $H(k)$  possesses the sublattice symmetry  $\mathcal{S} = \sigma_x$ , i.e.,  $\mathcal{S}H(k)\mathcal{S} = -H(k)$ . Furthermore, it also has the generalized particle-hole symmetry  $\mathcal{C} = \sigma_x$  and time-reversal symmetry  $\mathcal{T} = \sigma_0$ , in the sense that  $\mathcal{C}H^\top(k)\mathcal{C}^{-1} = -H(-k)$  and  $\mathcal{T}H^\top(k)\mathcal{T}^{-1} = H(-k)$ , where  $\top$  performs matrix transpo-

sition.  $H(k)$  thus belongs to an extension of the symmetry class BDI in the periodic table of non-Hermitian topological phases [14]. In the meantime,  $H(k)$  possesses the inversion symmetry  $\mathcal{P} = \sigma_z$  as  $\mathcal{P}H(k)\mathcal{P}^{-1} = H(-k)$ , which guarantees the correspondence between its bulk topological invariant  $w$  (as defined in Eq. (5)) and the number of Majorana edge modes under the open boundary condition [14].

According to Subsec. II A, the complex energy spectrum of LKC takes the form

$$E_{\pm}(k) = \pm\sqrt{h_y^2(k) + [h_z(k) - iv]^2} = \pm E(k), \quad (17)$$

which will become gapless when

$$\Delta \sin k = \pm v, \quad (18)$$

$$u + J \cos k = 0. \quad (19)$$

Combining these equations, we find the gapless quasimomenta

$$\pm k_0 = \pm \arccos(-u/J) \quad (20)$$

for  $|u| < |J|$ , and the boundary between different NHTPs as

$$\frac{u^2}{J^2} + \frac{v^2}{\Delta^2} = 1. \quad (21)$$

Geometrically, the trajectory of vector  $\mathbf{h}(k) \equiv [h_y(k), h_z(k)]$  forms an ellipse on the  $h_y$ - $h_z$  plane, which is centered at  $(0, u)$ . When the gapless condition Eq. (21) is satisfied, the spectrum  $E_{\pm}(k)$  hold a pair of EPs at  $(\pm v, 0)$  on the  $h_y$ - $h_z$  plane, which are passed through by the vector  $\mathbf{h}(k)$ . Whether the two EPs are encircled or not by the trajectory of  $\mathbf{h}(k)$  when  $k$  scans through the first BZ then distinguishes two possible NHTPs. With Eqs. (17) and (21), it is not hard to show that when  $u^2/J^2 + v^2/\Delta^2 < 1$  ( $> 1$ ), the two EPs are encircled (not encircled) by the trajectory of  $\mathbf{h}(k)$ . The topological invariant that distinguish these two phases has the form of Eq. (5), where the winding angle  $\phi(k)$  for the LKC is explicitly given by

$$\phi(k) = \arctan \left[ \frac{h_z(k) - iv}{h_y(k)} \right]. \quad (22)$$

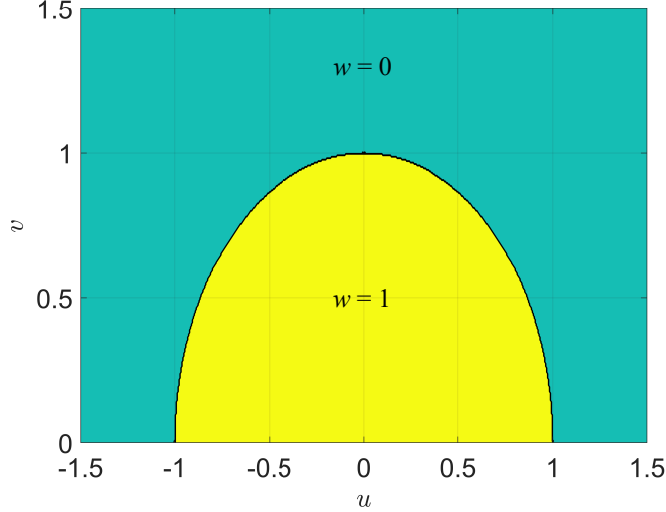


FIG. 1. Topological phase diagram of the LKC versus the real and imaginary parts of chemical potential  $u$  and  $v$ . Other system parameters are chosen as  $J = \Delta = 1$ . Each region with a uniform color denotes a NHTP, with the value of winding number  $w$  denoted explicitly therein.

In Fig. 1, we show the topological phase diagram of the LKC versus the real and imaginary parts of chemical potential  $u$  and  $v$ , with  $J = \Delta = 1$ . The winding numbers Eq. (5) of the non-Hermitian topological and trivial phases are found to be  $w = 1$  and  $w = 0$  for  $u^2/J^2 + v^2/\Delta^2 < 1$  and  $> 1$ , respectively. A loss-induced topological phase transition, which is unique to non-Hermitian systems, can be observed with the increase of  $v$ .

To link the NHTPs of LKC with the DQPTs, we employ the protocol introduced in Subsec. IIB, with the initial state  $\rho_0 = \sigma_0/2$  and the dynamics being governed by the Hamiltonian  $H(k)$  in Eq. (15). According to Eq. (6), the return amplitude at a later time  $t > 0$  is given by  $G(k, t) = \cos[E(k)t]$ , where  $E(k)$  is the dispersion relation of LKC in Eq. (17). From Eqs. (9) and (7), we find the critical momenta and times to be

$$\pm k_c = \pm \arccos(-u/J) = \pm k_0, \quad (23)$$

$$t_n(\pm k_c) = \left(n - \frac{1}{2}\right) \frac{\pi}{|\Delta| \sqrt{1 - (u^2/J^2 + v^2/\Delta^2)}}. \quad (24)$$

It is clear that when  $u^2/J^2 + v^2/\Delta^2 < 1$ , there are real solutions of  $t_n(k_c)$  for all  $n \in \mathbb{Z}$ , and the two critical momenta  $\pm k_c$  are coincide with the gapless quasimomenta  $\pm k_0$ , yielding the same critical period  $T(k_c) = \pi/\sqrt{\Delta^2(1 - u^2/J^2) - v^2}$ . On the other hand, there is no critical momenta and  $t_n$  is always imaginary when  $u^2/J^2 + v^2/\Delta^2 > 1$ , yielding no DQPTs at any real time  $t$ . When  $u^2/J^2 + v^2/\Delta^2 = 1$ , which corresponds to a gapless post-quench

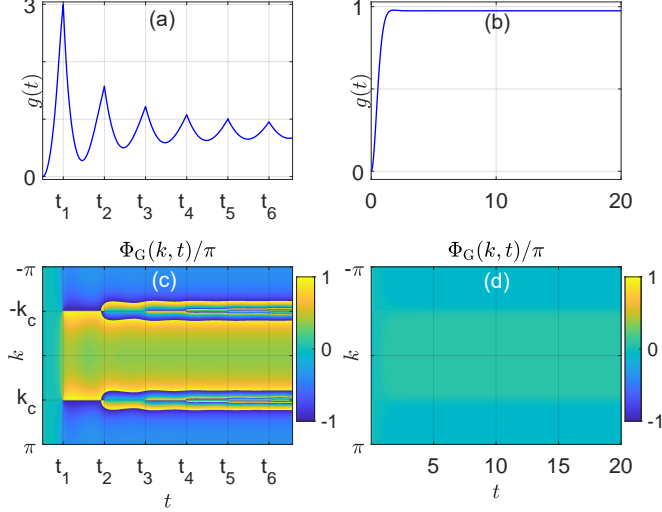


FIG. 2. Rate function of return probability  $g(t)$  [77] and noncyclic geometric phase  $\Phi_G(k, t)$  of the LKC model. Panels (a) and (c) present the case with system parameters  $J = \Delta = 1$ ,  $u = 0$  and  $v = 0.3$ , in which the winding number  $w = 1$  (topological phase) and DQPTs are observed as the cusps in  $g(t)$ . The critical momenta  $\pm k_c$  and critical times  $t_n$  ( $n = 1, \dots, 6$ ) are obtained from Eqs. (23) and (24). An extra  $2\pi$ -jump of the geometric phase  $\Phi_G(k, t)$  is observed at  $\pm k_c$  every time when the evolution of the system passes through a critical time  $t_n$ . Panels (b) and (d) present the case with system parameters  $J = \Delta = 1$ ,  $u = 0$  and  $v = 1.3$ , where there are no DQPTs and the winding number  $w = 0$  (trivial phase).

phase, we will have  $t_n(k_c) \rightarrow \infty$  for any solutions of critical momenta  $\pm k_c$ , and the resulting DQPTs are not observable. For completeness, we numerically compute the return rates and geometric phases with the help of Eqs. (10) and (11) for the cases with and without DQPTs in Fig. 2(a,c) and 2(b,d), respectively. As expected, DQPTs are only observed when the system is quenched to a nontrivial NHTP with the winding number  $w = 1$ .

Combining the analysis in this subsection, we obtain a *one-to-one correspondence* between the NHTPs and DQPTs in the LKC, which is summarized in Table I. This connection not only unifies the NHTPs and DQPTs in the system, but also provides a way to dynamically distinguishing the different NHTPs of LKC and detecting the gapless quasimomenta, as exemplified by Figs. 2(a,c).

## B. The lossy Kitaev chain with next-nearest-neighbor hoppings and pairings

We next consider the LKC with NNN hoppings and pairings, which could possess NHTPs with larger topological invariants. In the momentum space and Nambu spinor basis, the NNN LKC is described by the Hamiltonian  $H = \frac{1}{2} \sum_{k \in \text{BZ}} \Psi_k^\dagger H(k) \Psi_k$ , where  $H(k)$

Condition	Geometric picture	Winding number	Critical time and momenta
$\frac{u^2}{J^2} + \frac{v^2}{\Delta^2} < 1$	Two EPs are encircled by $\mathbf{h}(k)$	$w = 1$	DQPTs at $t_n(k_c)$ $\forall n \in \mathbb{Z}, k_c = k_0$
$\frac{u^2}{J^2} + \frac{v^2}{\Delta^2} = 1$	Two EPs are crossed by $\mathbf{h}(k)$	/	/
$\frac{u^2}{J^2} + \frac{v^2}{\Delta^2} > 1$	No EPs are encircled by $\mathbf{h}(k)$	$w = 0$	No $k_c$ and $t_n$ No DQPTs

TABLE I. The connection between NHTPs and DQPTs of the LKC model. The notation “/” in the table means “ill-defined”.  $k_0$  refers to the gapless quasimomenta of the model.

takes the same form as Eq. (15), with

$$\begin{aligned}
h_y(k) &= \Delta_1 \sin k + \Delta_2 \sin 2k, \\
h_z(k) &= u + J_1 \cos k + J_2 \cos 2k.
\end{aligned} \tag{25}$$

Here  $u$  is the real part of chemical potential,  $(J_1, \Delta_1)$  and  $(J_2, \Delta_2)$  are the nearest-neighbor and next-nearest-neighbor hopping and pairing amplitudes, respectively. It is not hard to verify that the  $H(k)$  here belongs to the same symmetry class as the LKC, with the same set of time-reversal, particle-hole, sublattice and inversion symmetries. The dispersion relations  $E_{\pm}(k)$  of  $H(k)$  share the same form with Eq. (17), yielding the gapless conditions

$$\Delta_1 \sin k + \Delta_2 \sin 2k = \pm v, \tag{26}$$

$$u + J_1 \cos k + J_2 \cos 2k = 0. \tag{27}$$

By solving Eq. (27), we could obtain at most four possible gapless quasimomenta  $\pm k_0^{\pm}$  as

$$\pm k_0^{\pm} = \pm \arccos \left[ \frac{-J_1 \pm \sqrt{J_1^2 + 8J_2(J_2 - u)}}{4J_2} \right]. \tag{28}$$

According to Eq. (26), the boundary between different NHTPs is then determined by

$$\sin k_0^{\pm} (\Delta_1 + 2\Delta_2 \cos k_0^{\pm}) = \pm v. \tag{29}$$

The explicit expression of the phase boundary in terms of system parameters is tedious, and will be left for numerical calculations. Geometrically, the trajectory of real vector

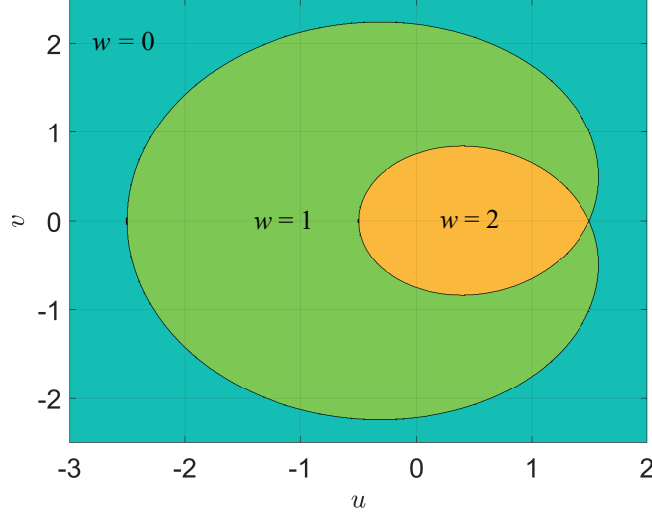


FIG. 3. Topological phase diagram of the NNN LKC model versus the real and imaginary parts of chemical potential  $u$  and  $v$ . Other system parameters are chosen as  $J_1 = \Delta_1 = 1$  and  $J_2 = \Delta_2 = 1.5$ . Each region with a uniform color corresponds to a NHTP, with the value of topological winding number  $w$  denoted explicitly therein. The black line separating different regions is the phase boundary obtained from Eq. (29).

$\mathbf{h}(k) = [h_y(k), h_z(k)]$  has the shape of a centered trochoid, which could encircle the two EPs of  $E(k)$  at  $(\pm v, 0)$  twice, once or zero times when  $k$  is scanned over the first BZ. These three possibilities then distinguish three different NHTPs, which are characterized by the topological winding number  $w$  in Eq. (5). In Fig. 3, we present the topological phase diagram of the NNN LKC model versus the real and imaginary parts of chemical potential  $u$  and  $v$ , with other system parameters set as  $J_1 = \Delta_1 = 1$  and  $J_2 = \Delta_2 = 1.5$ . The three topological phases are discriminated by different colored regions in the figure, with the phase boundary curve (black solid line) determined by Eq. (29), and the value of  $w$  denoted explicitly within each phase. The quantized changes of  $w$  with the increase of the lossy strength  $v$  again signify non-Hermiticity induced topological phase transitions in the system.

To build the connection between the NHTPs and the DQPTs of NNN LKC, we again employ the protocol introduced in Subsec. IIB, with the initial state  $\rho_0 = \sigma_0/2$  and the dynamics being governed by the Hamiltonian  $H(k)$  of the NNN LKC. The return amplitude at a later time  $t > 0$  is then given by  $G(k, t) = \cos[E(k)t]$ , with  $E(k)$  being the dispersion

Condition	Geometric picture	Winding number	Critical times and momenta
$h_y^2(k_c^\pm) > v^2$	Two EPs are encircled twice by $\mathbf{h}(k)$	$w = 2$	DQPTs at $t_n(k_c^\pm)$ $\forall n \in \mathbb{Z}, k_c^\pm = k_0^\pm$
$h_y^2(k_c^{+/-}) > v^2$ & $h_y^2(k_c^{-/+}) < v^2$	Two EPs are encircled once by $\mathbf{h}(k)$	$w = 1$	DQPTs at $t_n(k_c^{+/-})$ $\forall n \in \mathbb{Z}, k_c^\pm = k_0^\pm$
$h_y^2(k_c^\pm) < v^2$	No EPs are encircled by $\mathbf{h}(k)$	$w = 0$	No $k_c$ and $t_n$ No DQPTs

TABLE II. The connection between NHTPs and DQPTs of the NNN LKC model.

of NNN LKC. The critical momenta and time are further obtained from Eqs. (9) and (7) as

$$\pm k_c^\pm = \pm \arccos \left[ \frac{-J_1 \pm \sqrt{J_1^2 + 8J_2(J_2 - u)}}{4J_2} \right] = \pm k_0^\pm, \quad (30)$$

$$t_n(k_c^\pm) = \left( n - \frac{1}{2} \right) \frac{\pi}{\sqrt{(\Delta_1 \sin k_c^\pm + \Delta_2 \sin 2k_c^\pm)^2 - v^2}}, \quad (31)$$

where  $n \in \mathbb{Z}$ . In parallel with the discussions of Subsec. III A, we could summarize the relationship between NHTPs and DQPTs in the NNN LKC model by Table II. Again, we obtain a one-to-one correspondence between these two nonequilibrium phenomena, which also provides us with a way to detect NHTPs with large winding numbers and to locate the phase boundaries between them.

For completeness, we present three numerical examples for the DQPTs in the NNN LKC in Fig. 4. The system parameters are chosen as  $J_1 = \Delta_1 = 1$ ,  $J_2 = \Delta_2 = 1.5$ ,  $u = 0.5$  and  $v = 0.4, 1.4, 2.4$  for figure panels 4(a,d), 4(b,e) and 4(c,f). In Figs. 4(a,d) the post-quench system is in a NHTP with  $w = 2$ , and DQPTs are observed at two different sets of critical periods  $T(k_c^\pm) = \pi/\sqrt{h_y^2(k_c^\pm) - v^2}$  of  $g(t)$  in Fig. 4(a), with the two pairs of critical momenta  $\pm k_c^\pm$  given by Eq. (30) and imaged by the  $2\pi$ -jumps of geometric phase  $\Phi_G(k, t)$  in Fig. 4(d). In Figs. 4(b,e), the post-quench system is in a NHTP with  $w = 1$ , and DQPTs are repeated at only one critical period  $T(k_c^+) = \pi/\sqrt{h_y^2(k_c^+) - v^2}$  of  $g(t)$  in Fig. 4(b), with  $2\pi$ -jumps of geometric phase  $\Phi_G(k, t)$  observed at the critical momenta  $\pm k_c^+$  in Fig. 4(e). In Figs. 4(c,f), the post-quench system is in a trivial phase with  $w = 0$ , and no signatures of DQPTs are observed in the rate function  $g(t)$  and geometric phase  $\Phi_G(k, t)$ . Putting together, our numerical results confirm the connection between the NHTPs and DQPTs of the NNN LKC model, as summarized in Table II. Furthermore, the results presented here

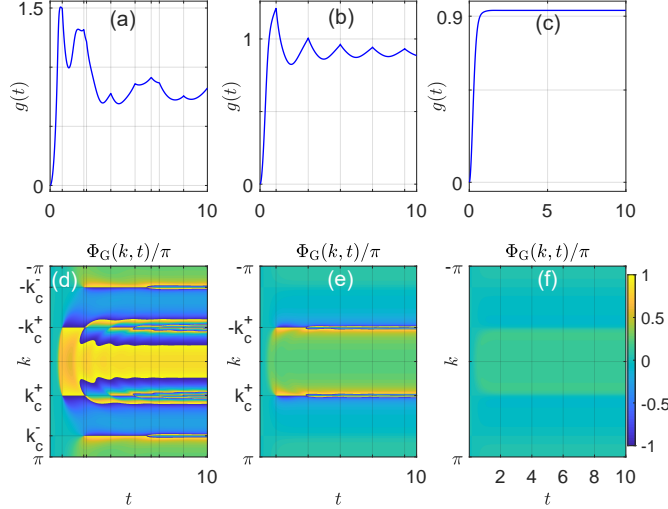


FIG. 4. The rate function  $g(t)$  in panels (a,b,c), and geometric phase  $\Phi_G(t)$  in panels (d,e,f) of the NNN LKC model [77]. The system parameters for the post-quench Hamiltonian are  $J_1 = \Delta_1 = 1$ ,  $J_2 = \Delta_2 = 1.5$ ,  $u = 0.5$ ,  $v = 0.4, 1.4$  and  $2.4$  in panels (a,d), (b,e) and (c,f), respectively. The winding numbers are  $w = 2, 1$  and  $0$  for the cases in panels (a,d), (b,e) and (c,f). DQPTs are observed as the cusps in  $g(t)$  in panels (a) and (b). In panels (a,d), the ticks along the horizontal axis denote the critical times  $t_1(k_c^+)$ ,  $t_1(k_c^-)$ ,  $t_2(k_c^+)$ ,  $t_3(k_c^+)$ ,  $t_4(k_c^+)$ ,  $t_2(k_c^-)$ ,  $t_5(k_c^+)$ ,  $t_6(k_c^+)$  from left to right, whose explicit values are obtained from Eqs. (30) and (31). In panels (b,e), the ticks along the horizontal axis are the critical times  $t_n(k_c^+)$  for  $n = 1, \dots, 5$  from left to right. An extra amount of  $2\pi$ -jump in the geometric phase  $\Phi_G(k, t)$  is observed at the corresponding critical momentum when a DQPT happens.

should be directly extendable to non-Hermitian models in the same symmetry class as the LKC, but with even longer-range hopping and pairing amplitudes.

### C. The nonreciprocal SSH model

In the last part of this section, we consider a nonreciprocal variant of the SSH model, which possesses a different set of symmetries compared with the LKC. In momentum representation, the Hamiltonian of NRSSH model takes the form  $H = \sum_{k \in \text{BZ}} \Psi_k^\dagger H(k) \Psi_k$ , where  $\Psi_k^\dagger = (a_k^\dagger, b_k^\dagger)$  is the creation operator on the two sublattices  $a$  and  $b$  of the SSH model, and  $k \in [-\pi, \pi)$  is the quasimomentum. The Bloch Hamiltonian  $H(k)$  is explicitly given by

$$H(k) = h_x(k)\sigma_x + [h_y(k) - i\gamma]\sigma_y, \quad (32)$$

with

$$h_x(k) = J_1 + J_2 \cos k, \quad h_y(k) = J_2 \sin k. \quad (33)$$

Here  $J_1 \pm \gamma$  and  $J_2$  are the intracell and intercell hopping amplitudes. A finite  $\gamma$  makes the intracell hopping asymmetric, leading to a non-Hermitian  $H(k)$ . From now on, we assume  $J_2, \gamma > 0$  without loss of generality. It is clear that the system possesses the sublattice symmetry  $\mathcal{S} = \sigma_z$ , in the sense that  $\mathcal{S}H(k)\mathcal{S} = -H(k)$ . This allows us to characterize the bulk topological phases of  $H(k)$  by the winding number  $w$ . Moreover,  $H(k)$  has the time reversal symmetry  $\mathcal{T} = \sigma_0$  and particle-hole symmetry  $\mathcal{C} = \sigma_z$ , i.e.,  $\mathcal{T}H^*(k)\mathcal{T}^{-1} = H(-k)$  and  $\mathcal{C}H^*(k)\mathcal{C}^{-1} = -H(-k)$ . Therefore, the NRSSH model belongs to the same BDI symmetry class as the Hermitian SSH model. Nevertheless,  $H(k)$  in Eq. (32) does not have the inversion symmetry of the Hermitian SSH model, but instead possesses the PT-symmetry, i.e.,  $\mathcal{P}\mathcal{T}H^*(k)(\mathcal{P}\mathcal{T})^{-1} = H(k)$ . This allows the bulk spectrum of  $H(k)$  to be very different under periodic and open boundary conditions, leading to the breakdown of conventional bulk-boundary correspondence [79].

The bulk spectrum of  $H(k)$  takes the form

$$E_{\pm}(k) = \pm\sqrt{h_x^2(k) + [h_y(k) - i\gamma]^2} = \pm E(k). \quad (34)$$

With Eq. (33), we see that the dispersion is gapless at zero energy when the following two conditions are met

$$J_1 \pm J_2 = \pm\gamma, \quad (35)$$

$$\sin k = 0, \quad (36)$$

which directly yield the phase boundary curves and the gapless quasimomenta  $k_0 = 0, \pi$ . Geometrically, the trajectory of vector  $\mathbf{h}(k) = [h_x(k), h_y(k)]$  forms a circle with radius  $J_2$  and centered at  $(J_1, 0)$  on the  $h_x$ - $h_y$  plane, while the EPs of the spectrum are located at  $(\pm\gamma, 0)$ . When  $J_1 - J_2 < -\gamma$  and  $J_1 + J_2 > \gamma$ , both two EPs are encircled by  $\mathbf{h}(k)$  when  $k$  scans over the first BZ. When  $J_1 - J_2 < -\gamma$  ( $J_1 + J_2 > \gamma$ ) and  $|J_1 + J_2| < \gamma$  ( $|J_1 - J_2| < \gamma$ ), the EP at  $(-\gamma, 0)$  ( $(\gamma, 0)$ ) is encircled by  $\mathbf{h}(k)$ . Otherwise no EPs are encircled by  $\mathbf{h}(k)$ . These three different situations distinguish three different types of bulk non-Hermitian topological phases, with each of them being characterized by the topological invariant  $w$  in Eq. (5), where the winding angle

$$\phi(k) = \arctan \left[ \frac{h_y(k) - i\gamma}{h_x(k)} \right]. \quad (37)$$

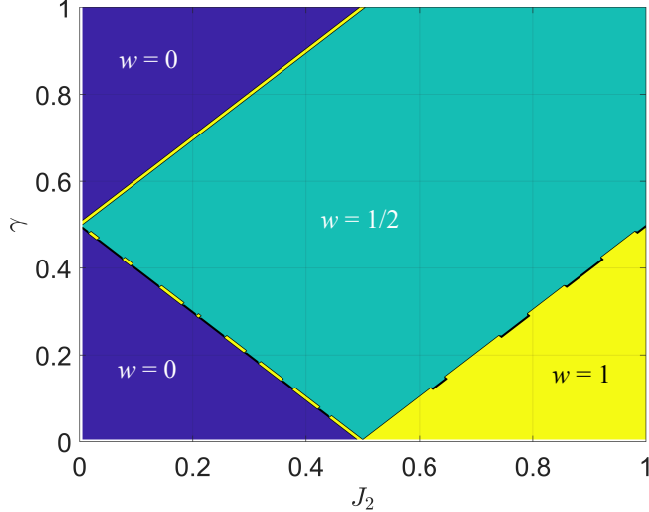


FIG. 5. Topological phase diagram of the NRSSH model versus the intercell hopping amplitude  $J_2$  and the asymmetric intracell modulation  $\gamma$ . The symmetric intracell hopping amplitude is set as  $J_1 = 0.5$ . Each regime with a uniform color corresponds to a NHTP, within which the topological winding number  $w$  takes a constant value as shown in the figure. The lines separating different NHTPs are phase boundaries obtained from Eq. (35).

In Fig. 5, we present the topological phase diagram of the NRSSH model versus the intercell hopping amplitude  $J_2$  and asymmetric hopping parameter  $\gamma$ , with the intracell hopping amplitude  $J_1 = 0.5$ . Each colored region in the phase diagram corresponds to a NHTP, with the value of topological winding number  $w$  denoted therein. The phase boundaries separating different regions are determined by Eq. (35). Despite non-Hermiticity-induced topological phase transitions, the NRSSH model also features a unique NHTP with winding number  $w = 1/2$ , which corresponds to the case in which only a single EP is encircled by  $\mathbf{h}(k)$ .

The connection between DQPTs and NHTPs in the NRSSH model can be built as follows. Choosing the initial state to be  $\rho_0 = \sigma_0/2$  as in Subsec. II B, the dynamics of the system at  $t > 0$  is governed by the Hamiltonian  $H(k)$  of the NRSSH model. The return amplitude at time  $t$  is given by  $G(k, t) = \cos[E(k)t]$ , with  $E(k)$  being the dispersion of  $H(k)$ . The critical

Condition	Geometric picture	Winding number	Critical times and momenta
$J_1 - J_2 < -\gamma$ & $J_1 + J_2 > \gamma$	Two EPs are encircled by $\mathbf{h}(k)$	$w = 1$	DQPTs at $t_n^{0,\pi}$ $\forall n \in \mathbb{Z}, k_c = 0, \pi$
$J_1 - J_2 < -\gamma$ & $ J_1 + J_2  < \gamma$ $J_1 + J_2 > \gamma$ & $ J_1 - J_2  < \gamma$	One EP is encircled by $\mathbf{h}(k)$	$w = 1/2$	DQPTs at $t_n^\pi$ $\forall n \in \mathbb{Z}, k_c = \pi$ DQPTs at $t_n^0$ $\forall n \in \mathbb{Z}, k_c = 0$
$ J_1 \pm J_2  < \gamma$ $ J_1 \pm J_2  > \gamma$	No EPs are encircled by $\mathbf{h}(k)$	$w = 0$	No $k_c$ and $t_n$ No DQPTs DQPTs at $t_n^{0,\pi}$ $\forall n \in \mathbb{Z}, k_c = 0, \pi$

TABLE III. The connection between NHTPs and DQPTs of the NRSSH model.

momenta and time are then obtained from Eqs. (9) and (7), i.e.,

$$k_c = (0, \pi) = k_0, \quad (38)$$

$$t_n(0) = \left(n - \frac{1}{2}\right) \frac{\pi}{\sqrt{(J_1 + J_2 - \gamma)(J_1 + J_2 + \gamma)}} \equiv t_n^0, \quad (39)$$

$$t_n(\pi) = \left(n - \frac{1}{2}\right) \frac{\pi}{\sqrt{(J_1 - J_2 - \gamma)(J_1 - J_2 + \gamma)}} \equiv t_n^\pi, \quad (40)$$

where  $n \in \mathbb{Z}$ . Combining these equations with the gapless conditions in Eqs. (35) and (36), we could immediately identify the relationship between NHTPs and DQPTs in the NRSSH model, as listed in Table III.

From the table, we observe that since there is only a single critical momentum for the NHTPs with  $w = 1/2$ , there is also a unique set of critical times ( $t_n^0$  or  $t_n^\pi$  for  $n \in \mathbb{Z}$ ) for the DQPTs in this case. This is in contrast with the NHTPs having  $w = 1$ , for which both  $k_c = k_0 = 0$  and  $\pi$  are the critical momenta, and DQPTs at two different critical time periods  $T(k_c = 0, \pi)$  are expected in the post-quench dynamics. In the meantime, we also observe an anomalous case as shown in the last row of Table III. In this case, DQPTs are found when the post-quench system is in a trivial phase with  $w = 0$ . Therefore, even though a nontrivial topological phase of the NRSSH model always lead to a unique set of DQPTs following the quench to that phase, the reverse is not true in general. Such a breakdown of the one-to-one correspondence between the DQPTs and NHTPs in the NRSSH model might be due to the absence of inversion symmetry, as compared with the situations in the LKC and its NNN extension. Nevertheless, the most intriguing phase of the NRSSH model, i.e.,

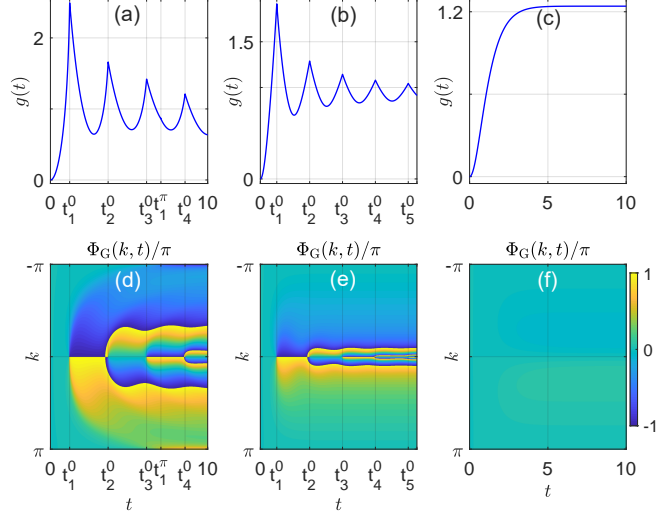


FIG. 6. The rate function  $g(t)$  [77] in panels (a,b,c), and geometric phase  $\Phi_G(t)$  in panels (d,e,f) of the NRSSH model. The system parameters for the post-quench Hamiltonian are  $J_1 = 0.5$ ,  $(J_2, \gamma) = (0.8, 0.2)$ ,  $(0.4, 0.5)$  and  $(0.2, 0.8)$  in panels (a,d), (b,e) and (c,f), respectively. The winding numbers are  $w = 1, 1/2$  and  $0$  for the cases in panels (a,d), (b,e) and (c,f). DQPTs are observed as the cusps in  $g(t)$  in panels (a) and (b). In panels (a,b,d,e), the ticks along the horizontal axis denote the critical times from left to right, whose explicit values are obtained from Eqs. (38)-(40). An extra amount of  $2\pi$ -jump in the geometric phase  $\Phi_G(k, t)$  is observed around the corresponding critical momentum in panels (d,e) when a DQPT happens.

the one with  $w = 1/2$  can still be distinguished from the other phases through the DQPTs. Therefore, the connection between NHTPs and DQPTs we discovered can still be used as a powerful tool to probe the details of the NHTPs in the NRSSH model.

For completeness, we present the DQPTs in three typical post-quench phases of the NRSSH model in Fig. 6. In Figs. 6(a,d), the post-quench phase has winding number  $w = 1$ , and DQPTs are observed as cusps in the rate function  $g(t)$  at two sets of critical times  $t_n^{0,\pi}$ . At each critical time, a  $2\pi$ -jump in the geometric phase  $\Phi_G(k, t)$  is observed at both the critical momenta  $k_c = 0, \pi$ . In Figs. 6(b,e), the post-quench phase has winding number  $w = 1/2$ , and DQPTs are found at a unique set of critical time  $t_n^0$ , where a  $2\pi$ -jump in the geometric phase  $\Phi_G(k, t)$  is observed around  $k_c = 0$ . In Figs. 6(c,f), the post-quench phase is trivial and no DQPTs are found in the post-quench dynamics. Putting together, we found that the NHTPs and DQPTs in the NRSSH model are also two closely related phenomena, and the later can be employed to dynamically probe the properties of the former.

#### IV. EXPERIMENTAL PROPOSAL

With all the theoretical and numerical results presented above, we now sketch an experimental proposal in which our predicted connection between NHTPs and DQPTs may be verified. Recently, a setup containing an NV center in diamond has been employed to realize the PT-symmetry breaking transition of a non-Hermitian two-level Hamiltonian [29]. The general idea is to dilate a PT-symmetric Hamiltonian into a Hermitian one, and execute the dynamics with the dilated Hamiltonian. Since all the three models discussed in the previous section possess two bulk bands together with the PT-symmetry, the setup proposed in Ref. [29] tends out to be an ideal platform in which the topological invariants and DQPTs of our systems can be detected.

The Hamiltonian we are interested in, as shown in Eq. (1) can be generally expressed as  $H(k) = \mathbf{d}(k) \cdot \boldsymbol{\sigma}$ , where  $\mathbf{d}(k) = [h_a(k) - ig_a(k), h_b(k) - ig_b(k)]$  and  $\boldsymbol{\sigma} = (\sigma_a, \sigma_b)$ . The strategy of Ref. [29] is to dilate  $H(k)$  into a Hermitian counterpart with the help of an ancilla qubit. The dilated Hamiltonian  $H'(k, t)$  yields the Schrödinger equation

$$i \frac{d}{dt} |\Omega(k, t)\rangle = H'(k, t) |\Omega(k, t)\rangle, \quad (41)$$

where  $|\Omega(k, t)\rangle$  denotes the state of the composite system. With an appropriate post-selection scheme, the measurement results can be restricted to a unique outcome for the ancilla qubit [29]. Within the scheme, the composite state  $|\Omega(k, t)\rangle$  takes the form

$$|\Omega(k, t)\rangle = |\Psi(k, t)\rangle |-\rangle + \omega(t) |\Psi(k, t)\rangle |+\rangle, \quad (42)$$

where  $\omega(t)$  is an appropriate linear operator, and the ancilla qubit basis  $|\pm\rangle$  are chosen to be the eigenstates of Pauli matrix  $\sigma_y$

$$|-\rangle = \frac{|0\rangle - i|1\rangle}{\sqrt{2}}, \quad |+\rangle = -i \frac{|0\rangle + i|1\rangle}{\sqrt{2}}. \quad (43)$$

In the experiment, a  $-\pi/2$  pulse is applied following the evolution, and only the measurement results inside the state manifold  $|\Psi(k, t)\rangle |-\rangle$  is post-selected.

The explicit form of dilated Hamiltonian  $H'(k, t)$  is not unique. A convenient choice

realized by the experiment in Ref. [29] is

$$H'(k, t) = \Lambda(k, t) \otimes \sigma_0 + \Gamma(k, t) \otimes \sigma_z, \quad (44)$$

where

$$\Lambda(k, t) = \left\{ H(k) + \left[ i \frac{d}{dt} \omega(t) + \omega(t) H(k) \right] \omega(t) \right\} M^{-1}(t), \quad (45)$$

$$\Gamma(k, t) = i \left[ H(k) \omega(t) - \omega(t) H(k) - i \frac{d}{dt} \omega(t) \right] M^{-1}(t), \quad (46)$$

with the time-dependent operator  $M(t) \equiv \omega^\dagger(t)\omega(t) + \sigma_0$ . Expanding  $\Lambda(k, t)$  and  $\Gamma(k, t)$  by the Pauli matrices  $\sigma_{x,y,z}$  and  $\sigma_0$ , we can further express  $H'(k, t)$  as

$$H'(k, t) = \sum_{i=0}^3 \sigma_i \otimes [A_i(k, t)\sigma_0 + B_i(k, t)\sigma_z], \quad (47)$$

where the real coefficients  $A_i(k, t)$  and  $B_i(k, t)$  for  $i = 0, 1, 2, 3$  can be obtained numerically [29].

Experimentally, the dilated Hamiltonian  $H'(k, t)$  contain four levels at each  $k$ , which can be encoded in the ground state manifold of electron and nuclear spins in an NV center. The dynamics of the system, in which  $H(k)$  takes the form of Eq. (15) or (32) can be monitored in the population of post-selected state, which further provides us with the information about DQPTs in the corresponding lattice model. The topological winding numbers of the model can also be obtained by measuring the dynamic winding number of time-averaged spin textures [47], as suggested in Ref. [43]. In a very recent experiment, the non-Hermitian topological phases of a nonreciprocal SSH model have been detected in an NV center setup following the universal dilation scheme [30], which confirms the applicability of the experimental proposal.

## V. SUMMARY

In this manuscript, we establish a relationship between NHTPs and DQPTs in 1D systems. DQPTs are found when the system is quenched from a trivial to a non-Hermitian topological phase. The numbers of critical momenta and the periods of critical time are further related to the topological invariants of the post-quench non-Hermitian phases. Our

results are demonstrated explicitly in three characteristic non-Hermitian lattice models, which possess non-Hermiticity induced topological phase transitions. Finally, we introduce a proposal to observe the connection between NHTPs and DQPTs by manipulating an NV center in diamond. This work therefore bridges the gap between two classes of fascinating nonequilibrium phenomena, the NHTPs and DQPTs, and brings new insights about the dynamical characterization of non-Hermitian states of matter.

In this work, our theory is applied to one-dimensional two-band models with chiral symmetry. Our initial attempts also suggest that the theoretical framework presented here is generalizable to chiral-symmetric multiple-band models [41, 78]. However, due to the complexity of multiple-band systems in the study of NHTPs and DQPTs, we expect that our theory would subject to appropriate modifications when it is applied to these systems. This interesting topic will be left for future explorations. In the meantime, it would be interesting to extend our findings to non-Hermitian systems under open boundary conditions, where the non-Hermitian skin effects and the breakdown of bulk-edge correspondence may have significant impact [79]. Furthermore, possible extensions of the connection between NHTPs and DQPTs to systems in other symmetry classes, higher spatial dimensions and with many-body interactions certainly deserve further explorations.

## ACKNOWLEDGEMENT

L.Z. is supported by the National Natural Science Foundation of China (Grant No. 11905211), the China Postdoctoral Science Foundation (Grant No. 2019M662444), the Fundamental Research Funds for the Central Universities (Grant No. 841912009), the Young Talents Project at Ocean University of China (Grant No. 861801013196), and the Applied Research Project of Postdoctoral Fellows in Qingdao (Grant No. 861905040009).

## Appendix A: Symmetry of the geometric phase

In this appendix, we analyze the symmetry of the geometric phase and its effect on the calculation of the dynamical topological order parameter (DTOP) for the three models considered in this work. Due to their chiral symmetries, the Hamiltonians of the three

models in Sec. III share the common formalism

$$H(k) = d_a(k)\sigma_a + d_b(k)\sigma_b, \quad (\text{A1})$$

where  $a, b = x, y, z$  and  $a \neq b$ . It can be equivalently written as

$$H(k) = E(k)\mathbf{n}(k) \cdot \boldsymbol{\sigma}, \quad (\text{A2})$$

where

$$E(k) = \sqrt{d_a^2(k) + d_b^2(k)}, \quad (\text{A3})$$

$$\mathbf{n}(k) = [n_a(k), n_b(k)] = \left[ \frac{d_a(k)}{E(k)}, \frac{d_b(k)}{E(k)} \right], \quad (\text{A4})$$

and  $\boldsymbol{\sigma} = (\sigma_a, \sigma_b)$ . It is clear that  $\mathbf{n}(k)$  is a unit vector with  $\mathbf{n}(k) \cdot \mathbf{n}(k) = 1$ .

According to Eqs. (6) and (12), the total phase of the return amplitude reads

$$\Phi(k, t) = -i \ln \left\{ \frac{\cos[E(k)t]}{|\cos[E(k)t]|} \right\}. \quad (\text{A5})$$

It is clear that  $\Phi(-k, t) = \Phi(k, t)$  once  $E(-k) = \pm E(k)$ . This is clearly the case for the models considered in Subsecs. III A and III B according to the expressions of their bulk spectrum  $E_{\pm}(k)$ . Instead, for the model studied in Subsec. III C, the total phase does not have the parity (inversion) symmetry.

To obtain the dynamical phase, we introduce the biorthogonal representation of non-Hermitian systems. In this representation, the right and left eigenvectors  $\{|\psi_s(k)\rangle | s = \pm\}$  and  $\{|\tilde{\psi}_s(k)\rangle | s = \pm\}$  of  $H(k)$  satisfy the eigenvalue equations

$$H(k)|\psi_s(k)\rangle = E_s(k)|\psi_s(k)\rangle \quad (\text{A6})$$

and

$$H^\dagger(k)|\tilde{\psi}_s(k)\rangle = E_s^*(k)|\tilde{\psi}_s(k)\rangle. \quad (\text{A7})$$

The Hamiltonian  $H(k)$  can also be expressed in this representation as

$$H(k) = \sum_{s=\pm} E_s(k)|\psi_s(k)\rangle\langle\tilde{\psi}_s(k)|. \quad (\text{A8})$$

The time-evolution operators in the spaces of right and left eigenvectors are

$$U(k, t) = \sum_{s=\pm} e^{-iE_s(k)t} |\psi_s(k)\rangle \langle \tilde{\psi}_s(k)| \quad (\text{A9})$$

and

$$\tilde{U}(k, t) = \sum_{s=\pm} e^{-iE_s(k)t} |\tilde{\psi}_s(k)\rangle \langle \psi_s(k)|, \quad (\text{A10})$$

respectively.

According to the definition of dynamical phase  $\Phi_D(k, t)$  in Eq. (13) of the main text, we have

$$\Phi_D(k, t) = - \int_0^t dt' \text{Re} \left\{ \frac{\text{Tr}[\tilde{U}^\dagger(k, t')U(k, t')H(k)]}{\text{Tr}[\tilde{U}^\dagger(k, t')U(k, t')]} \right\}. \quad (\text{A11})$$

With Eqs. (A9) and (A10), we can recast  $\Phi_D(k, t)$  into a more explicit form. The denominator of the integrand tends out to be

$$\text{Tr}[\tilde{U}^\dagger(k, t')U(k, t')] = 2 \cosh\{2\text{Im}[E(k)]t\}. \quad (\text{A12})$$

Furthermore, the numerator in the integrand of Eq. (A11) yields

$$\text{Tr}[\tilde{U}^\dagger(k, t')U(k, t')H(k)] = 2E(k) \sinh\{2\text{Im}[E(k)]t\}. \quad (\text{A13})$$

Putting together, we find the dynamical phase to be

$$\begin{aligned} \Phi_D(k, t) &= - \int_0^t dt' \text{Re}[E(k)] \tanh\{2\text{Im}[E(k)]t'\} \\ &= - \text{Re}[E(k)] \frac{\ln[\cosh\{2\text{Im}[E(k)]t\}]}{2\text{Im}[E(k)]}. \end{aligned} \quad (\text{A14})$$

Referring to the main text, we see that as  $E(-k) = E(k)$  for the LKC and NNN LKC models, we also have  $\Phi_D(-k, t) = \Phi_D(k, t)$  for these two models. Therefore, we conclude that the geometric phases  $\Phi_G(k, t) = \Phi(k, t) - \Phi_D(k, t)$  of the LKC and NNN LKC models in the main text both possess the inversion symmetry, i.e.,  $\Phi_G(-k, t) = \Phi_G(k, t)$ . This allows us to confine the range of integration to half of the first BZ, e.g.,  $k \in [0, \pi]$  for the calculation of dynamical topological order parameters in Eq. (14) for these two models. Comparatively, for the NRSSH model studied in Subsec. III C of the main text, we have

$\Phi_G(-k, t) \neq \Phi_G(k, t)$  since  $E(-k) \neq E(k)$ , and the whole first BZ  $k \in [-\pi, \pi]$  should be employed in the calculation of its dynamical topological order parameter. Experimentally, information about the geometric phase may be directly obtained by measuring the complex spectrum dispersion  $E(k)$  of the system [29].

## Appendix B: DTOP of the models

In this appendix, we present numerical results for the dynamical topological order parameter (DTOP) of the three models investigated in Sec. III of the main text. Since the geometric phase does not show any winding behaviors when there are no DQPTs, we will only consider the DTOP of the cases in which DQPTs are observed in the rate function of return probability.

For the LKC model defined in Subsec. III A, we present the DTOP  $\nu(t)$  versus time  $t$  in Fig. 7. The system parameters are the same as those used in Figs. 2(a) and 2(c), and the DTOP is calculated by Eq. (14) of the main text. We observe that every time when the evolution of the system passes through a critical time, the value of DTOP shows a quantized jump  $|\Delta\nu(t)| = 1$ , which signifies the appearance of a DQPT. Meanwhile, we also notice that  $\nu(t)$  may not take quantized values between certain pairs of critical times (e.g., for  $t \in (t_1, t_2)$ ), which might be due to our choice of reduced BZ  $k \in [0, \pi]$  in the calculation of  $\nu(t)$ . Nevertheless, the quantized jump of DTOP across each critical time already provides us with essential information about the drastic topological change of the system when undergoing a DQPT.

For the NNN LKC model defined in Subsec. III B, we show the DTOP  $\nu(t)$  versus time  $t$  in Fig. 8. The system parameters are chosen to be the same as those used in Figs. 4(a,d) and 4(b,e), and the DTOP is calculated by Eq. (14) of the main text. We also notice that the value of DTOP shows a quantized jump  $|\Delta\nu(t)| = 1$  every time when the system evolves through a critical time, which indicates the existence of a DQPT. The applicability of DTOP to the LKC and NNN LKC models also highlights its universality in characterizing the DQPTs of 1D non-Hermitian systems with chiral symmetry.

For the NRSSH model defined in Subsec. III C, we present the DTOP  $\nu(t)$  versus time  $t$  in Fig. 9. The system parameters are set as the same as those used in Figs. 6(a,d) and 4(b,e), and the DTOP is calculated by Eq. (14) of the main text. We find again the quantized

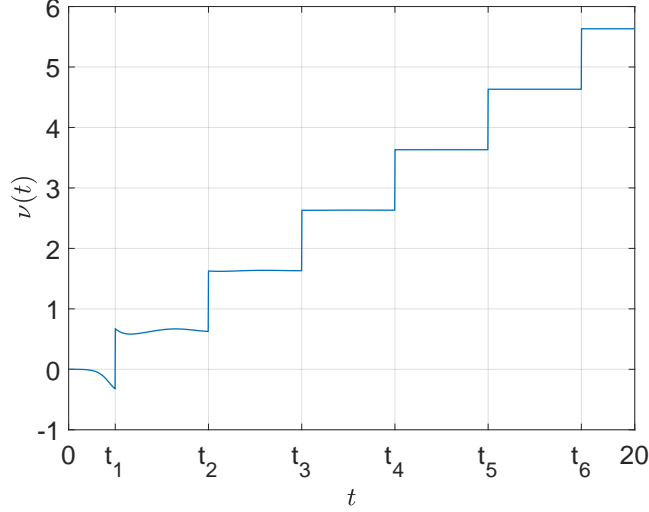


FIG. 7. DTOP  $\nu(t)$  of the LKC (blue solid line). System parameters are  $J = \Delta = 1$ ,  $u = 0$  and  $v = 0.3$ , in which the winding number  $w = 1$  (topological phase), and DQPTs are observed when the values of  $\nu(t)$  possess quantized jumps. The critical times  $t_n$  ( $n = 1, \dots, 6$ ) are obtained from Eq. (24) in the main text.

jump of DTOP every time when the system evolves across a critical time, implying the existence of a DQPT. Furthermore, the values of DTOP remain quantized between any pair of the critical times, which is expected as the whole Brillouin zone  $k \in [-\pi, \pi]$  is used in the calculation of  $\nu(t)$ . Besides, we also notice that the value of DTOP changes monotonically in time when the post-quench system has a half-quantized winding number  $w = 1/2$ , which is consistent with the connection between the exceptional non-Hermitian topology and DQPTs as first observed in Ref. [52].

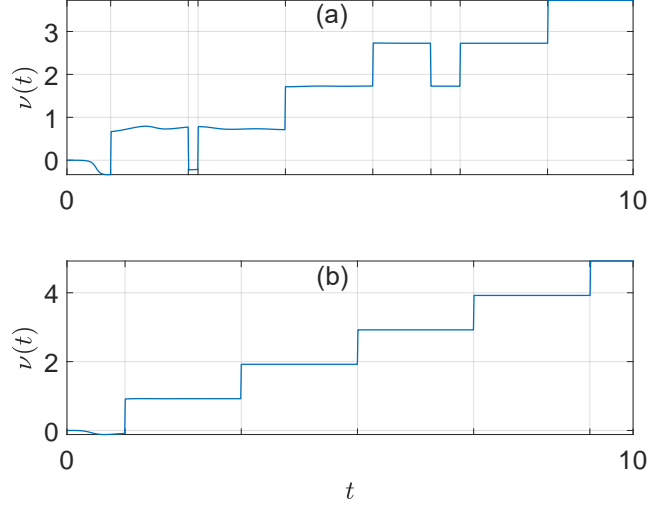


FIG. 8. DTOP  $\nu(t)$  of the NNN LKC model versus time. The system parameters for the post-quench Hamiltonian are  $J_1 = \Delta_1 = 1$ ,  $J_2 = \Delta_2 = 1.5$ ,  $u = 0.5$ ,  $v = 0.4$  and  $1.4$  in panels (a) and (b), respectively. The winding numbers are  $w = 2$  and  $1$  for the cases in panels (a) and (b). DQPTs are observed when  $\nu(t)$  possesses quantized jumps in panels (a) and (b). In panel (a), the ticks along the horizontal axis denote the critical times  $t_1(k_c^+)$ ,  $t_1(k_c^-)$ ,  $t_2(k_c^+)$ ,  $t_3(k_c^+)$ ,  $t_4(k_c^+)$ ,  $t_2(k_c^-)$ ,  $t_5(k_c^+)$ ,  $t_6(k_c^+)$  from left to right, whose explicit values are obtained from Eq. (31). In panel (b), the ticks along the horizontal axis are the critical times  $t_n(k_c^+)$  for  $n = 1, \dots, 5$  from left to right.

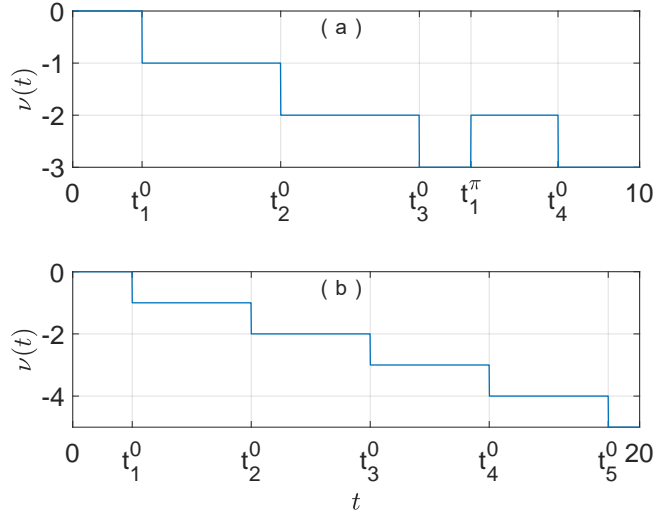


FIG. 9. DTOP  $\nu(t)$  of the NRSSH model versus time  $t$ . The system parameters for the post-quench Hamiltonian are  $J_1 = 0.5$ ,  $(J_2, \gamma) = (0.8, 0.2)$  and  $(0.4, 0.5)$  in panels (a) and (b), respectively. The winding numbers are  $w = 1$  and  $1/2$  for the cases in panels (a) and (b). DQPTs are observed when the values of  $\nu(t)$  possess quantized jumps in panels (a) and (b). In both panels, the ticks along the horizontal axis denote the critical times from left to right, whose explicit values are obtained from Eqs. (38)-(40).

- 
- [1] T. Yoshida, R. Peters, N. Kawakami, and Y. Hatsugai, Exceptional band touching for strongly correlated systems in equilibrium, *Prog. Theor. Exp. Phys.* **2020**, 12A109 (2020).
- [2] E. J. Bergholtz, J. C. Budich, and F. K. Kunst, Exceptional Topology of Non-Hermitian Systems, arXiv:1912.10048.
- [3] A. Ghatak and T. Das, New topological invariants in non-Hermitian systems, *J. Phys.: Condens. Matter* **31**, 263001 (2019).
- [4] K. Yokomizo and S. Murakami, Non-Bloch Band Theory and Bulk-Edge Correspondence in Non-Hermitian Systems, *Prog. Theor. Exp. Phys.* **2020**, 12A102 (2020).
- [5] Y. Ashida, Z. Gong, and M. Ueda, Non-Hermitian Physics, arXiv:2006.01837.
- [6] R. El-Ganainy, K. G. Makris, M. Khajavikhan, Z. H. Musslimani, S. Rotter and D. N. Christodoulides, Non-Hermitian physics and PT symmetry, *Nat. Phys.* **14**, 11-19 (2018).
- [7] V. V. Konotop, J. Yang, and D. A. Zezyulin, Nonlinear waves in PT-symmetric systems, *Rev. Mod. Phys.* **88**, 035002 (2016).
- [8] V. M. M. Alvarez, J. E. B. Vargas, M. Berdakin, and L. E. F. Foa Torres, Topological states of non-Hermitian systems, *Eur. Phys. J. Special Topics* **227**, 1295 (2018).
- [9] J. Doppler, A. A. Mailybaev, J. Böhm, U. Kuhl, A. Girschik, F. Libisch, T. J. Milburn, P. Rabl, N. Moiseyev, and S. Rotter, Dynamically encircling an exceptional point for asymmetric mode switching, *Nature (London)* **537**, 76 (2016).
- [10] A. U. Hassan, B. Zhen, M. Soljačić, M. Khajavikhan, and D. N. Christodoulides, Dynamically Encircling Exceptional Points: Exact Evolution and Polarization State Conversion, *Phys. Rev. Lett.* **118**, 093002 (2017).
- [11] X.-L. Zhang, S. Wang, B. Hou, and C. T. Chan, Dynamically Encircling Exceptional Points: In situ Control of Encircling Loops and the Role of the Starting Point, *Phys. Rev. X* **8**, 021066 (2018).
- [12] H. Shen, B. Zhen, and L. Fu, Topological Band Theory for Non-Hermitian Hamiltonians, *Phys. Rev. Lett.* **120**, 146402 (2018).
- [13] Z. Gong, Y. Ashida, K. Kawabata, K. Takasan, S. Higashikawa, and M. Ueda, Topological Phases of Non-Hermitian Systems, *Phys. Rev. X* **8**, 031079 (2018).
- [14] K. Kawabata, K. Shiozaki, M. Ueda, and M. Sato, Symmetry and Topology in Non-Hermitian

- Physics, Phys. Rev. X **9**, 041015 (2019).
- [15] H. Zhou and J. Y. Lee, Periodic table for topological bands with non-Hermitian symmetries, Phys. Rev. B **99**, 235112 (2019).
- [16] W. Gou, T. Chen, D. Xie, T. Xiao, T.-S. Deng, B. Gadway, W. Yi, and B. Yan, Tunable Nonreciprocal Quantum Transport through a Dissipative Aharonov-Bohm Ring in Ultracold Atoms, Phys. Rev. Lett. **124**, 070402 (2020).
- [17] J. Li, A. K. Harter, J. Liu, L. d. Melo, Y. N. Joglekar, and L. Luo, Observation of parity-time symmetry breaking transitions in a dissipative Floquet system of ultracold atoms, Nat. Commun. **10**, 855 (2019).
- [18] Y. Xu, S.-T. Wang, and L.-M. Duan, Weyl Exceptional Rings in a Three-Dimensional Dissipative Cold Atomic Gas, Phys. Rev. Lett. **118**, 045701 (2017).
- [19] J.M. Zeuner, M.C. Rechtsman, Y. Plotnik, Y. Lumer, S. Nolte, M.S. Rudner, M. Segev, and A. Szameit, Observation of a Topological Transition in the Bulk of a Non-Hermitian System. Phys. Rev. Lett. **115**, 040402 (2015).
- [20] S. Weimann, M. Kremer, Y. Plotnik, Y. Lumer, S. Nolte, K. G. Makris, M. Segev, M. C. Rechtsman, and A. Szameit, Topologically protected bound states in photonic parity-time-symmetric crystals, Nat. Mater. **16**, 433-438 (2017).
- [21] K. Wang, X. Qiu, L. Xiao, X. Zhan, Z. Bian, B. C. Sanders, W. Yi, and P. Xue, Observation of emergent momentum-time skyrmions in parity-time-symmetric non-unitary quench dynamics, Nat. Commun. **10**, 2293 (2019).
- [22] L. Xiao, T. Deng, K. Wang, G. Zhu, Z. Wang, W. Yi, and P. Xue, Non-Hermitian bulk-boundary correspondence in quantum dynamics, Nat. Phys. **16**, 761-766 (2020).
- [23] T. Hofmann, T. Helbig, F. Schindler, N. Salgo, M. Brzezińska, M. Greiter, T. Kiessling, D. Wolf, A. Vollhardt, A. Kabaši, C. H. Lee, A. Bilušić, R. Thomale, and T. Neupert, Reciprocal skin effect and its realization in a topoelectrical circuit, Phys. Rev. Res. **2**, 023265 (2020).
- [24] T. Helbig, T. Hofmann, S. Imhof, M. Abdelghany, T. Kiessling, L. W. Molenkamp, C. H. Lee, A. Szameit, M. Greiter, and R. Thomale, Generalized bulk-boundary correspondence in non-Hermitian topoelectrical circuits, Nat. Phys. **16**, 747-750 (2020).
- [25] S. Liu, S. Ma, C. Yang, L. Zhang, W. Gao, Y. J. Xiang, T. J. Cui, and S. Zhang, Gain- and Loss-Induced Topological Insulating Phase in a Non-Hermitian Electrical Circuit, Phys. Rev. Appl. **13**, 014047 (2020).

- [26] W. Zhu, X. Fang, D. Li, Y. Sun, Y. Li, Y. Jing, and H. Chen, Simultaneous Observation of a Topological Edge State and Exceptional Point in an Open and Non-Hermitian Acoustic System, *Phys. Rev. Lett.* **121**, 124501 (2018).
- [27] C. Shen, J. Li, X. Peng, and S. A. Cummer, Synthetic exceptional points and unidirectional zero reflection in non-Hermitian acoustic systems, *Phys. Rev. Mater.* **2**, 125203 (2018).
- [28] H. Gao, H. Xue, Q. Wang, Z. Gu, T. Liu, J. Zhu, and B. Zhang, Observation of topological edge states induced solely by non-Hermiticity in an acoustic crystal, *Phys. Rev. B* **101**, 180303(R) (2020).
- [29] Y. Wu, W. Liu, J. Geng, X. Song, X. Ye, C.-K. Duan, X. Rong, and J. Du, Observation of parity-time symmetry breaking in a single-spin system, *Science* **364**, 878-880 (2019).
- [30] W. Zhang, X. Ouyang, X. Huang, X. Wang, H. Zhang, Y. Yu, X. Chang, Y. Liu, D.-L. Deng, and L.-M. Duan, Observation of non-Hermitian topology with non-unitary dynamics of solid-state spins, arXiv:2012.09191.
- [31] Z. Lin, H. Ramezani, T. Eichelkraut, T. Kottos, H. Cao, and D. N. Christodoulides, Unidirectional Invisibility Induced by PT-Symmetric Periodic Structures, *Phys. Rev. Lett.* **106**, 213901 (2011).
- [32] L. Feng, Y.-L. Xu, W. S. Fegadolli, M.-H. Lu, J. E. B. Oliveira, V. R. Almeida, Y.-F. Chen, and A. Scherer, Experimental demonstration of a unidirectional reflectionless parity-time metamaterial at optical frequencies, *Nat. Mater.* **12**, 108 (2013).
- [33] G. Harari, M.A. Bandres, Y. Lumer, M.C. Rechtsman, Y.D. Chong, M. Khajavikhan, D.N. Christodoulides, and M. Segev, Topological insulator laser: Theory. *Science* **359**, 4003 (2018).
- [34] M.A. Bandres, S. Wittek, G. Harari, M. Parto, J. Ren, M. Segev, D.N. Christodoulides, and M. Khajavikhan, Topological insulator laser: Experiments. *Science* **359**, 4005 (2018).
- [35] Y. V. Kartashov and D. V. Skryabin, Two-Dimensional Topological Polariton Laser, *Phys. Rev. Lett.* **122**, 083902 (2019).
- [36] J. Wiersig, Enhancing the Sensitivity of Frequency and Energy Splitting Detection by Using Exceptional Points: Application to Microcavity Sensors for Single-Particle Detection, *Phys. Rev. Lett.* **112**, 203901 (2014).
- [37] H.-K. Lau and A. A. Clerk, Fundamental limits and non-reciprocal approaches in non-Hermitian quantum sensing, *Nat. Commun.* **9**, 4320 (2018).
- [38] H. Hodaei, A. U. Hassan, S. Wittek, H. Garcia-Gracia, R. El-Ganainy, D. N. Christodoulides,

- and M. Khajavikhan, Enhanced sensitivity at higher-order exceptional points, *Nature* **548**, 187-191 (2017).
- [39] W. Chen, S. K. Özdemir, G. Zhao, J. Wiersig, and L. Yang, Exceptional points enhance sensing in an optical microcavity, *Nature* **548**, 192-196 (2017).
- [40] L. Zhou and J. Pan, Non-Hermitian Floquet topological phases in the double-kicked rotor, *Phys. Rev. A* **100**, 053608 (2019).
- [41] L. Zhou, Non-Hermitian Floquet phases with even-integer topological invariants in a periodically quenched two-leg ladder, *Entropy* **22**, 746 (2020).
- [42] J. Pan and L. Zhou, Non-Hermitian Floquet second order topological insulators in periodically quenched lattices, *Phys. Rev. B* **102**, 094305 (2020).
- [43] B. Zhu, Y. Ke, H. Zhong and C. Lee, Dynamic winding number for exploring band topology, *Phys. Rev. Res.* **2**, 023043 (2020).
- [44] L. Zhou and J. Gong, Non-Hermitian Floquet topological phases with arbitrarily many real-quasienergy edge states, *Phys. Rev. B* **98**, 205417 (2018).
- [45] L. Zhou, Dynamical characterization of non-Hermitian Floquet topological phases in one dimension, *Phys. Rev. B* **100**, 184314 (2019).
- [46] L. Zhou, Y. Gu and J. Gong, Dual topological characterization of non-Hermitian Floquet phases, *Phys. Rev. B* **103**, L041404 (2021).
- [47] L. Zhang, L. Zhang, S. Niu, and X.-J. Liu, Dynamical classification of topological quantum phases, *Sci. Bull.* **63**, 1385 (2018).
- [48] M. Heyl, Dynamical quantum phase transitions: a review, *Rep. Prog. Phys.* **81** 054001 (2018).
- [49] M. Heyl, Dynamical quantum phase transitions: A brief survey, *EPL* **125** 26001 (2019).
- [50] A. A. Zvyagin, Dynamical quantum phase transitions (Review Article), *Low Temp. Phys.* **42**, 971 (2016).
- [51] N. Sedlmayr, Dynamical Phase Transitions in Topological Insulators, *Acta Physica Polonica A* **135**, 1191 (2019).
- [52] L. Zhou, Q.-h. Wang, H. Wang, and J. Gong, Dynamical quantum phase transitions in non-Hermitian lattices, *Phys. Rev. A* **98**, 022129 (2018).
- [53] M. Heyl, A. Polkovnikov, and S. Kehrein, Dynamical Quantum Phase Transitions in the Transverse-Field Ising Model, *Phys. Rev. Lett.* **110**, 135704 (2013).
- [54] F. Pollmann, S. Mukerjee, A. G. Green, and J. E. Moore, Dynamics after a sweep through a

- quantum critical point, *Phys. Rev. E* **81**, 020101(R) (2010).
- [55] P. Uhrich, N. Defenu, R. Jafari, and J. C. Halimeh, Out-of-equilibrium phase diagram of long-range superconductors, *Phys. Rev. B* **101**, 245148 (2020).
- [56] N. Fläschner, D. Vogel, M. Tarnowski, B. S. Rem, D.-S. Lühmann, M. Heyl, J. C. Budich, L. Mathey, K. Sengstock, and C. Weitenberg, Observation of dynamical vortices after quenches in a system with topology, *Nat. Phys.* **14**, 265 (2018).
- [57] S. Smale, P. He, B. A. Olsen, K. G. Jackson, H. Sharum, S. Trotzky, J. Marino, A. M. Rey, and J. H. Thywissen, Observation of a transition between dynamical phases in a quantum degenerate Fermi gas, *Sci. Adv.* **5**, eaax1568 (2018).
- [58] H.-X. Yang, T. Tian, Y.-B. Yang, L.-Y. Qiu, H.-Y. Liang, A.-J. Chu, C. B. Dağ, Y. Xu, Y. Liu, and L.-M. Duan, Observation of dynamical quantum phase transitions in a spinor condensate, *Phys. Rev. A* **100**, 013622 (2019).
- [59] T. Tian, H.-X. Yang, L.-Y. Qiu, H.-Y. Liang, Y.-B. Yang, Y. Xu, and L.-M. Duan, Observation of Dynamical Quantum Phase Transitions with Correspondence in an Excited State Phase Diagram, *Phys. Rev. Lett.* **124**, 043001 (2020).
- [60] P. Jurcevic, H. Shen, P. Hauke, C. Maier, T. Brydges, C. Hempel, B. P. Lanyon, M. Heyl, R. Blatt, and C. F. Roos, Direct Observation of Dynamical Quantum Phase Transitions in an Interacting Many-Body System, *Phys. Rev. Lett.* **119**, 080501 (2017).
- [61] J. Zhang, G. Pagano, P. W. Hess, A. Kyprianidis, P. Becker, H. Kaplan, A. V. Gorshkov, Z.-X. Gong, and C. Monroe, Observation of a many-body dynamical phase transition with a 53-qubit quantum simulator, *Nature (London)* **551**, 601 (2017).
- [62] X. Guo, C. Yang, Y. Zeng, Y. Peng, H. Li, H. Deng, Y. Jin, S. Chen, D. Zheng, and H. Fan, Observation of Dynamical Quantum Phase Transition by a Superconducting Qubit Simulation, *Phys. Rev. Appl.* **11**, 044080 (2019).
- [63] T. Tian, Y. Ke, L. Zhang, S. Lin, Z. Shi, P. Huang, C. Lee, and J. Du, Observation of dynamical phase transitions in a topological nanomechanical system, *Phys. Rev. B* **100**, 024310 (2019).
- [64] K. Wang, X. Qiu, L. Xiao, X. Zhan, Z. Bian, W. Yi, and P. Xue, Simulating Dynamic Quantum Phase Transitions in Photonic Quantum Walks, *Phys. Rev. Lett.* **122**, 020501 (2019).
- [65] X.-Y. Xu, Q.-Q. Wang, M. Heyl, J. C. Budich, W.-W. Pan, Z. Chen, M. Jan, K. Sun, J.-S. Xu, Y.-J. Han, C.-F. Li, and G.-C. Guo, Measuring a Dynamical Topological Order Parameter in Quantum Walks, *Light: Science & Applications* **9**, 7 (2020).

- [66] K. Yang, L. Zhou, W. Ma, X. Kong, P. Wang, X. Qin, X. Rong, Y. Wang, F. Shi, J. Gong, and J. Du, Floquet dynamical quantum phase transitions, *Phys. Rev. B* **100**, 085308 (2019).
- [67] A. Kosior and K. Sacha, Dynamical quantum phase transitions in discrete time crystals, *Phys. Rev. A* **97**, 053621 (2018).
- [68] A. Kosior, A. Syrwid, and K. Sacha, Dynamical quantum phase transitions in systems with broken continuous time and space translation symmetries, *Phys. Rev. A* **98**, 023612 (2018).
- [69] S. Zamani, R. Jafari, and A. Langari, Floquet dynamical quantum phase transition in the extended XY model: Nonadiabatic to adiabatic topological transition, *Phys. Rev. B* **102**, 144306 (2020).
- [70] R. Jafari and A. Akbari, Floquet dynamical phase transition and entanglement spectrum, *Phys. Rev. A* **103**, 012204 (2021).
- [71] L. Zhou, Floquet dynamical quantum phase transitions in periodically quenched systems, arXiv:2011.00199.
- [72] S. Vajna and B. Dóra, Topological classification of dynamical phase transitions, *Phys. Rev. B* **91**, 155127 (2015).
- [73] J. C. Budich and M. Heyl, Dynamical topological order parameters far from equilibrium, *Phys. Rev. B* **93**, 085416 (2016).
- [74] L. Pastori, S. Barbarino, and J. C. Budich, Signatures of topology in quantum quench dynamics and their interrelation, *Phys. Rev. Res.* **2**, 033259 (2020).
- [75] T. V. Zache, N. Mueller, J. T. Schneider, F. Jendrzejewski, J. Berges, and P. Hauke, Dynamical Topological Transitions in the Massive Schwinger Model with a  $\theta$ -Term, *Phys. Rev. Lett.* **122**, 050403 (2019).
- [76] U. Bhattacharya, S. Bandyopadhyay, and A. Dutta, Mixed state dynamical quantum phase transitions, *Phys. Rev. B* **96**, 180303(R) (2017).
- [77] Numerically, we computed a normalized  $g(t)$  in order to cancel the changing norm of the evolving state. Such a normalization will not affect the critical times and momenta DQPTs predicted by the theory.
- [78] Y. He and C.-C. Chien, Non-Hermitian generalizations of extended Su-Schrieffer-Heeger models, *J. Phys.: Condens. Matter* **33** 085501 (2020).
- [79] S. Yao and Z. Wang, Edge States and Topological Invariants of Non-Hermitian Systems, *Phys. Rev. Lett.* **121**, 086803 (2018).